01 Jul 2014

Spatially Continuous Distributed Fiber Optic Sensing using Optical Carrier Based Microwave Interferometry

Jie Huang
Missouri University of Science and Technology, jieh@mst.edu

Xinwei Lan

Ming Luo

Hai Xiao
Missouri University of Science and Technology, xiaoha@mst.edu

Recommended Citation

J. Huang et al., "Spatially Continuous Distributed Fiber Optic Sensing using Optical Carrier Based Microwave Interferometry," *Optics Express*, vol. 22, no. 15, pp. 18757-18769, Optical Society of America, Jul 2014.
The definitive version is available at https://doi.org/10.1364/OE.22.018757

Spatially continuous distributed fiber optic sensing using optical carrier based microwave interferometry

Jie Huang,[1] Xinwei Lan,[1] Ming Luo[2] and Hai Xiao[1,*]

[1]*The Holcombe Department of Electrical and Computer Engineering, Center for Optical Materials Science and Engineering Technologies (COMSET), Clemson University, 105 Riggs Hall, Clemson, SC, 29634, USA*
[2]*Habsonic LLC, 1105 Hauck Drive, Rolla, MO 65401, USA*
[*]*haix@clemson.edu*

Abstract: This paper reports a spatially continuous distributed fiber optic sensing technique using optical carrier based microwave interferometry (OCMI), in which many optical interferometers with the same or different optical path differences are interrogated in the microwave domain and their locations can be unambiguously determined. The concept is demonstrated using cascaded weak optical reflectors along a single optical fiber, where any two arbitrary reflectors are paired to define a low-finesse Fabry-Perot interferometer. While spatially continuous (i.e., no dark zone), fully distributed strain measurement was used as an example to demonstrate the capability, the proposed concept may also be implemented on other types of waveguide or free-space interferometers and used for distributed measurement of various physical, chemical and biological quantities.

OCIS codes: (060.2310) Fiber optics; (060.2370) Fiber optics sensors; (120.3180) Interferometry; (060.5625) Radio frequency photonics.

References and links

1. K. Grattan and T. Sun, "Fiber optic sensor technology: an overview," Sens. Actuators A Phys. **82**(1–3), 40–61 (2000).
2. A. D. Kersey, T. A. Berkoff, and W. W. Morey, "Multiplexed fiber Bragg grating strain-sensor system with a fiber Fabry - Perot wavelength filter," Opt. Lett. **18**(16), 1370–1372 (1993).
3. K. O. Hill and G. Meltz, "Fiber Bragg grating technology fundamentals and overview," J. Lightwave Technol. **15**(8), 1263–1276 (1997).
4. Y. Wang, J. Gong, B. Dong, W. Bi, and A. Wang, "A quasi-distributed sensing network with time-division-multiplexed fiber Bragg gratings," IEEE Photon. Technol. Lett. **23**(2), 70–72 (2011).
5. B. A. Childers, M. E. Froggatt, S. G. Allison, T. C. Moore Sr, D. A. Hare, C. F. Batten, and D. C. Jegley, "Use of 3000 Bragg grating strain sensors distributed on four 8-m optical fibers during static load tests of a composite structure," Proc. SPIE **4332**, 133 (2001).
6. J. L. Brooks, R. H. Wentworth, R. C. Youngquist, M. Tur, B. Y. Kim, and H. Shaw, "Coherence multiplexing of fiber-optic interferometric sensors," J. Lightwave Technol. **3**(5), 1062–1072 (1985).
7. J. Wang, B. Dong, E. Lally, J. Gong, M. Han, and A. Wang, "Multiplexed high temperature sensing with sapphire fiber air gap-based extrinsic Fabry-Perot interferometers," Opt. Lett. **35**(5), 619–621 (2010).
8. F. Shen and A. Wang, "Frequency-estimation-based signal-processing algorithm for white-light optical fiber Fabry-Perot interferometers," Appl. Opt. **44**(25), 5206–5214 (2005).
9. J. Huang, L. Hua, X. Lan, T. Wei, and H. Xiao, "Microwave assisted reconstruction of optical interferograms for distributed fiber optic sensing," Opt. Express **21**(15), 18152–18159 (2013).
10. B. Sutapun, M. Tabib-Azar, and A. Kazemi, "Pd-coated elastooptic fiber optic Bragg grating sensors for multiplexed hydrogen sensing," Sens. Actuators B Chem. **60**(1), 27–34 (1999).
11. L. Chen, T. Li, C. C. Chan, R. Menon, P. Balamurali, M. Shaillender, B. Neu, X. Ang, P. Zu, W. Wong, and K. C. Leong, "Chitosan based fiber-optic Fabry–Perot humidity sensor," Sens. Actuators B Chem. **169**, 167–172 (2012).
12. M. Froggatt and J. Moore, "High-spatial-resolution distributed strain measurement in optical fiber with Rayleigh scatter," Appl. Opt. **37**(10), 1735–1740 (1998).
13. Y. Koyamada, M. Imahama, K. Kubota, and K. Hogari, "Fiber-optic distributed strain and temperature sensing with very high measurand resolution over long range using coherent OTDR," J. Lightwave Technol. **27**(9), 1142–1146 (2009).
14. X. Bao, J. Dhliwayo, N. Heron, D. J. Webb, and D. A. Jackson, "Experimental and theoretical studies on a distributed temperature sensor based on Brillouin scattering," J. Lightwave Technol. **13**(7), 1340–1348 (1995).

#212236 - $15.00 USD Received 15 May 2014; revised 15 Jul 2014; accepted 18 Jul 2014; published 25 Jul 2014

15. J. Dakin, D. Pratt, G. Bibby, and J. Ross, "Distributed optical fibre Raman temperature sensor using a semiconductor light source and detector," Electron. Lett. **21**(13), 569–570 (1985).
16. M. N. Alahbabi, Y. T. Cho, and T. P. Newson, "150-km-range distributed temperature sensor based on coherent detection of spontaneous Brillouin backscatter and in-line Raman amplification," J. Opt. Soc. Am. B **22**(6), 1321–1324 (2005).
17. K. Shimizu, T. Horiguchi, Y. Koyamada, and T. Kurashima, "Coherent self-heterodyne Brillouin OTDR for measurement of Brillouin frequency shift distribution in optical fibers," J. Lightwave Technol. **12**(5), 730–736 (1994).
18. W. Eickhoff and R. Ulrich, "Optical frequency domain reflectometry in single-mode fiber," Appl. Phys. Lett. **39**(9), 693–695 (1981).
19. M. A. Soto, G. Bolognini, F. Di Pasquale, and L. Thévenaz, "Simplex-coded BOTDA fiber sensor with 1 m spatial resolution over a 50 km range," Opt. Lett. **35**(2), 259–261 (2010).
20. Y. Dong, L. Chen, and X. Bao, "Time-division multiplexing-based BOTDA over 100 km sensing length," Opt. Lett. **36**(2), 277–279 (2011).
21. J. Huang, X. Lan, H. Wang, L. Yuan, and H. Xiao, "Optical carrier-based microwave interferometers for sensing application," Proc. SPIE **9098**, 90980H (2014).
22. J. Capmany and D. Novak, "Microwave photonics combines two worlds," Nat. Photon. **1**(6), 319–330 (2007).
23. J. Yao, "Microwave photonics," J. Lightwave Technol. **27**(3), 314–335 (2009).
24. K. Bisshopp and D. Drucker, "Large deflection of cantilever beams," Q. Appl. Math. **3**, 273–275 (1945).

1. Introduction

In the past few decades, optical fibers have been widely used for various sensing applications due to their low loss, light weight, immunity to electromagnetic interference (EMI), and resistance to corrosion [1]. One of the most attractive features of optical fiber sensing is its capability of measurement of spatially distributed parameters. In general, optical fiber based distributed sensing can be implemented either by multiplexing a large number of discrete sensors to form a spatially-distributed measurement network or by sending a pulsed signal to probe the spatially-resolved information as a function of time-of-arrival.

In multiplexed sensing, or the so-called quasi-distributed sensing, many discrete sensors are cascaded in series along a single optical fiber. The signals of the sensors are unambiguously demodulated either in time or frequency domain. For example, fiber Bragg gratings (FBGs) have been cascaded along a single fiber for multiplexed sensing. The cascaded FBGs can have different Bragg wavelengths so that their spectral shifts can be unambiguously determined [2, 3]. Thousands of weakly reflecting FBGs can also be made of the same resonant wavelength and interrogated using either optical time domain reflectormetry (OTDR) [4] or optical frequency domain reflectometry (OFDR) [5]. In addition to FBGs, fiber optic interferometers (FOIs) can also be multiplexed [6]. For example, fiber Fabry-Perot interferometers (FPIs) of different cavity lengths have been multiplexed onto a single fiber. Identification of the cascaded FPIs can be achieved by Fourier transform of the optical interferogram in the spectral domain to obtain their individual optical path differences [7, 8]. Recently, it has been demonstrated that cascaded FPIs with the same or similar cavity lengths can be discriminated using microwave assisted separation and reconstruction of the individual optical interferograms in the spectrum domain [9]. One unique feature of the multiplexed sensing is that each point sensor along the optical fiber can be flexibly encoded to measure different physical, chemical and biological quantities [10, 11]. However, the aforementioned multiplexed sensing techniques were still quasi-distributed or spatially interrupted, only providing discrete sampling of the space, leaving dark zones among the sensors.

Spatially continuous measurement can be achieved by collecting the back-scattered signals generated by the elastic (e.g., Rayleigh) [12, 13] or inelastic (e.g., Brillouin or Raman) [14–16] scatterings along the fiber. Optical probing and collection of these back-scattered signals have been done in the time domain through OTDR [17] or in the frequency domain using OFDR [18]. The unique advantage of the scattering based distributed sensing is the spatial continuity (no dark-zones). For example, long-range spatially continuous Brillouin optical time-domain analysis (BOTDA) measurement systems has been demonstrated using both methods [19, 20]. Another advantage of the back-scattering based distributed sensing is that it does not necessarily require extra modifications to the optical fiber, making it possible to cover a long measurement distance (e.g., tens of kilometers). Most of the quantitative

#212236 - $15.00 USD Received 15 May 2014; revised 15 Jul 2014; accepted 18 Jul 2014; published 25 Jul 2014

measurements based on scattering have been performed using singlemode fibers. The back-scattered signals in an optical fiber are mainly sensitive to strain and temperature.

Recently, we demonstrated a new concept of optical carrier based microwave interferometry (OCMI) [21] inspired by the research advancements in microwave photonics [22, 23]. By interrogating optical interferometers in microwave domain, the OCMI concept integrates the strengths of optics and microwave, providing several unique features that are particularly advantageous for sensing applications. These features include low dependent on the types of optical waveguides, insensitive to variations in optical polarizations, high signal quality, relieved fabrication requirements, and the potential capability for distributed sensing.

In this paper, we report our studies on using the OCMI technique for spatially continuous distributed sensing. Intrinsic FPIs formed by cascaded weak reflectors in an optical fiber are used for the purpose of demonstration. It is expected that the proposed technique can also be used for multiplexing other types of fiber interferometers. Distributed strain sensing is used as an example in this paper. However, we believe that the interferometry based system can be easily modified for distributed measurement of other physical, chemical and biological parameters.

2. Concept of the spatially continuous distributed sensing based on cascaded OCMI-FPIs

Figure 1 illustrates the fundamental concept of the spatially continuous distributed sensing technique using cascaded inline OCMI-FPIs. The essence of OCMI is to read an optical interferometer in microwave domain as described in [21].

As shown in Fig. 1, the light from a broadband optical source is intensity-modulated by a microwave signal whose frequency can be scanned via computer control. The microwave-modulated light, where the optical is the carrier and the microwave is the envelope, is then sent into (via a fiber optic circulator) an optical fiber with cascaded weak reflectors. The optical reflections travel backwards, pass the fiber circulator and are detected by a high-speed photodetector. The optical detection is synchronized with the microwave frequency by a phase lock loop (PLL) so that the amplitude and phase of the reflected signal can be resolved. After scanning the microwave frequency through the entire available range, the reflection spectrum (with both amplitude and phase) is obtained.

The inverse complex Fourier transform of the reflection spectrum provides the time-resolved discrete reflections along the optical fiber. A time gating function with two opening windows is then applied to the time series so as to "cut out" two arbitrary reflections (e.g., Γ_i and Γ_j in Fig. 1) while suppressing other values to zero. These two reflections are then Fourier transformed back to frequency domain to reconstruct a microwave interferogram, which can be used to find the optical path difference (OPD) between the two reflectors (e.g., d_{ij}). The change in the OPD between these two reflectors (e.g., Δd_{ij}) can be calculated based on the frequency shift of the microwave interferogram.

#212236 - $15.00 USD Received 15 May 2014; revised 15 Jul 2014; accepted 18 Jul 2014; published 25 Jul 2014

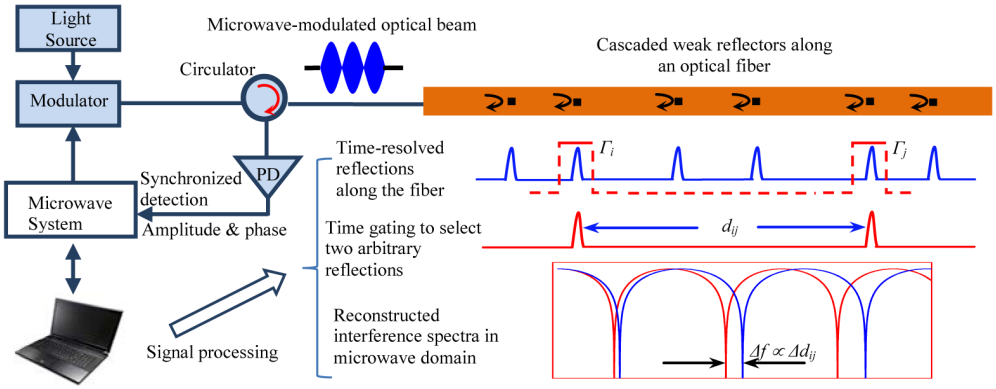

Fig. 1. Schematic illustration of the fundamental concept of the spatially continuous distributed sensing using cascaded FPIs. The segmentation is achieved by implementing a time-gating function with two windows to isolate two arbitrary reflections (e.g., Γ_i and Γ_j) for reconstruction of the microwave interferogram, whose spectral shift is proportional to the length change of the segment between the i-*th* and j-*th* reflectors (i.e., Δd_{ij}).

Because any two reflectors can be chosen to form an OCMI interferogram, spatially continuous distributed sensing can be realized by consecutively selecting two adjacent reflectors along the cable. In addition, the base length of the interferometer can be varied by choosing any two arbitrary reflectors (e.g., select 2 and 5 and suppress the other reflectors). As such, the gauge length can be flexibly reconfigured during measurement.

3. Modeling and simulations

Let's start with an optical wave in the form of

$$E_o = A\exp\{-j[\omega t+\varphi]\} \tag{1}$$

where t is the time; E_o is the electric field; A is the amplitude; φ is the phase; ω is the angular optical frequency.

The microwave signal used to modulate the optical wave is given by

$$s(t) = M\cos(\Omega t+\phi) \tag{2}$$

where M is the amplitude of the modulation, which falls in the range of 0 to 1, Ω is the microwave angular frequency, and ϕ is the phase.

The electric field of the light wave modulated by the microwave becomes

$$E = m(t)E_o \tag{3}$$

where $m(t)$ is the amplitude modulation term, given by

$$m(t) = \sqrt{1+s(t)} = \sqrt{1+M\cos(\Omega t+\phi)} \tag{4}$$

The microwave-modulated light, in which the optical is the carrier and the microwave is the envelope, is then sent into an optical fiber with cascaded reflectors. The reflection of each reflector can be designed to be weak enough so that the light can be transmitted over many sensors and the multiple reflections are negligible. The electric field of the total reflected light wave is given by

$$E_{total} = \sum_{i=1}^{N} E_i(t,z_i) = \sum_{i=1}^{N} m_i(t,z_i)E_{o,i}(t,z_i) \tag{5}$$

#212236 - $15.00 USD Received 15 May 2014; revised 15 Jul 2014; accepted 18 Jul 2014; published 25 Jul 2014

where N is the total number of the reflectors; z_i represents the location of the i-*th* reflector. Note that in Eq. (5), both the optical and microwave components are functions of the locations (z_i) of the reflectors.

The optical component (i.e., the electric field of the i-*th* optical reflection) in Eq. (5) is given by

$$E_{o,i}(t,z_i)=\Gamma_i A\exp\left\{-j\left[\omega\left(t+\frac{2z_i n}{c}\right)\right]\right\} \tag{6}$$

where Γ_i is the amplitude reflection coefficient of the i-*th* reflector seen by the photodetector; c is the speed of light in vacuum; n is the effective refractive index.

The microwave amplitude modulation term in Eq. (5) is

$$m(t,z_i)=\sqrt{1+M\cos\left[\Omega\left(t+\frac{W}{c}+\frac{2z_i n}{c}\right)\right]} \tag{7}$$

where the microwave envelopes include two delay terms. The first is the delay associated with the common electrical length (W) of the microwave system and this delay is the same for all the paths. The second delay term is the contribution from the optical propagation delays at different reflectors.

For simplicity, let's assume that the broadband optical source has a rectangular shaped spectrum in the frequency range from ω_{min} to ω_{max}. The total power of the superimposed optical waves of all the reflections is given by

$$\begin{aligned}\left|E_{total}\right|^2&=\frac{1}{\Delta\omega}\int_{\omega_{\min}}^{\omega_{\max}}\left|\sum_{i=1}^{N}E_i(t,z_i)\right|^2 d\omega\\&=\frac{1}{\Delta\omega}\left(\int_{\omega_{\min}}^{\omega_{\max}}\sum_{i=1}^{N}\left|E(t,z_i)\right|^2 d\omega+\int_{\omega_{\min}}^{\omega_{\max}}\sum_{i=1,j=1,i\neq j}^{N}\left[E(t,z_i)E^*(t,z_j)+E^*(t,z_i)E(t,z_j)\right]d\omega\right)\end{aligned} \tag{8}$$

where the first integral is the self-product term and the second integral is the cross-product term, and $\Delta\omega=\omega_{\max}-\omega_{\min}$.

Let's first examine the cross-product term in Eq. (8)

$$\begin{aligned}&\frac{1}{\Delta\omega}\int_{\omega_{\min}}^{\omega_{\max}}\sum_{i=1,j=1,i\neq j}^{N}\left[E(t,z_i)E^*(t,z_j)+E^*(t,z_i)E(t,z_j)\right]d\omega\\&=\frac{2}{\Delta\omega}\sum_{i=1,j=1,i\neq j}^{N}m(t,z_i)m(t,z_j)\Gamma_i\Gamma_j A^2\int_{\omega_{\min}}^{\omega_{\max}}\left\{\cos\left[\frac{2\omega}{c}(z_1-z_2)n\right]\right\}d\omega\end{aligned} \tag{9}$$

It is interesting to notice that the cross-product term is the optical interference signal similar to a conventional all-optical interferometer. In the OCMI, the optical path difference (OPD) is chosen to be sufficiently larger than the coherence length of the optical source, i.e., $(z_1-z_2)n>>c/\Delta\omega$. Under this condition, the integral term in Eq. (9) approaches zero. In our experimental OCMI system, we used a light source with a spectral width of 50 nm at the center wavelength of about 1550 nm, whose coherence length was about 48 μm. A typical OCMI has an OPD of a few centimeters that is much larger than the coherence length of a broadband light source. As a result, the contribution from pure optical interference as depicted in Eq. (9) is negligible in a typical OCMI system.

The self-product term in Eq. (8) is found to be

#212236 - $15.00 USD Received 15 May 2014; revised 15 Jul 2014; accepted 18 Jul 2014; published 25 Jul 2014

$$\frac{1}{\Delta\omega}\int_{\omega_{\min}}^{\omega_{\max}}\sum_{i=1}^{N}\left|E\left(t,z_i\right)\right|^2 d\omega=\sum_{i=1}^{N}\Gamma_i^2A^2+\sum_{i=1}^{N}\Gamma_i^2A^2M\cos\left[\Omega\left(t+\frac{W}{c}+\frac{2z_in}{c}\right)\right] \quad (10)$$

which includes a DC term and the summation of a series of sinusoids at the microwave frequency of Ω .

The OCMI system uses synchronized detection to eliminate the DC term (first term) and record the amplitude and phase of the microwave signal (second term) in Eq. (10). As a result, the total signal after optoelectronic conversion by the photodetector (with a gain of g) and synchronized microwave detection is given by

$$S=A_{eff}\cos\left(\Omega t+\Phi_{eff}\right) \quad (11)$$

In Eq. (11), A_{eff} and Φ_{eff} are the amplitude and phase of the microwave signal, respectively.

$$A_{eff}=g\sqrt{\sum_{i,j}^{N}A_{eff,i}A_{eff,j}\cos\left(\phi_{eff,i}-\phi_{eff,j}\right)}$$

$$\Phi_{eff}=\arctan\left[\frac{\sum_{i}^{N}\Gamma_i^2\sin\left[\Omega\left(\frac{W}{c}+\frac{2z_in}{c}\right)\right]}{\sum_{i,j}^{N}\Gamma_i^2\cos\left[\Omega\left(\frac{W}{c}+\frac{2z_in}{c}\right)\right]}\right],\quad \Phi_{eff}\in\left\{-\pi,\pi\right\}$$

where

$$A_{eff,i}=\Gamma_i^2A^2M,$$
$$A_{eff,j}=\Gamma_j^2A^2M$$
$$\phi_{eff,i}=\Gamma_i^2A^2M\left(\frac{W}{c}+\frac{2z_in}{c}\right)$$
$$\phi_{eff,j}=\Gamma_j^2A^2M\left(\frac{W}{c}+\frac{2z_jn}{c}\right)$$

After scanning the microwave frequency through the entire available range (from Ω_{min} to Ω_{max}), the complex microwave reflection spectrum (with both amplitude and phase) is obtained. By applying a complex and inverse Fourier-transform to the microwave spectrum, a series of cardinal sine functions are obtained at discrete reflectors, given by:

$$\begin{aligned}\mathrm{X}\left(t\right)&=\frac{1}{2\pi}\int_{\Omega_{\min}}^{\Omega_{\max}}S\exp\left(j\Omega t\right)d\Omega\\&=\frac{1}{2\pi}\int_{\Omega_{\min}}^{\Omega_{\max}}\sum_{i=1}^{N}\Gamma_i^2A^2M\cos\left[\Omega\left(t+\frac{W}{c}+\frac{2z_in}{c}\right)\right]\exp\left(j\Omega t\right)d\Omega\\&=\sum_{i=1}^{N}\Gamma_i^2A^2M\left|\sin c\left[\left(\Omega_{\max}-\Omega_{\min}\right)\left(t+\tau_i\right)\right]\right|\end{aligned} \quad (12)$$

where $\tau_i=\frac{W}{c}+\frac{2z_in}{c}$ is the propagation delay of the signal corresponding to the *i-th* reflector.

In Eq. (12), the maximum amplitudes of the discrete sinc functions are proportional to the reflectivity of the cascaded reflectors. In addition, Eq. (12) also provides the location information of the reflectors along the optical fiber. The peaks of the sinc functions are at the

#212236 - $15.00 USD Received 15 May 2014; revised 15 Jul 2014; accepted 18 Jul 2014; published 25 Jul 2014

specific reflector locations (z_i) that can be found when the delays (τ_i) are determined. The frequency bandwidth (Ω_{max} -Ω_{min}) determines the spatial resolution, i.e., the minimum distance between two adjacent reflectors to avoid an overlap of the two pulses in the time domain. The larger the microwave bandwidth, the narrower is the pulse width (sinc function) in time domain and the higher is the spatial resolution.

A time gating function with two windows is then applied to time domain signal given in Eq. (12) so as to isolate two arbitrary reflections. The gate functions could be designed to have different shapes such as rectangular, Hanning, Turkey, etc. Here we generalize the gate function as *g(t)*. The time domain signal after applying a gate function is thus given by *X(t)g(t)*. The gated signal is then Fourier transformed back to the frequency domain to reconstruct the microwave interferogram, which can be used to find the optical distance between the two reflectors (e.g., d_{ij}). The reconstructed OCMI-FPI interferogram is thus given by

$$S_{OCMI} = S * G(\Omega)\exp(-i\Omega\tau_0) \tag{13}$$

where *G(Ω)* is the inverse Fourier transform of the gate function *g(t)*; τ_0 is the time delay of the gate function. As shown in Eq. (13), the reconstructed microwave FPI interferogram in spectrum domain is in essence a convolution of the microwave signal *S* and *G(Ω)*. Here we define the optical path difference (OPD) of the OCMI-FPI is

$$OPD = d_{ij} = \left|2\left(z_i - z_j\right)n\right| \tag{14}$$

The free spectral range (FSR) of the reconstructed interference spectrum is a function of the OPD, given by

$$FSR = \frac{c}{OPD} \tag{15}$$

Similar to an optical interference spectrum, the microwave amplitude spectrum in the reconstructed OMCI-FPI can be used to find the OPD of an interferometer. It can also be used to find the change in OPD based on the interference fringe shift.

Numerical simulations were performed to gain an intuitive understanding of using the OCMI technique for distributed sensing. In the simulation, the fiber used was a Corning SMF-28e singlemode fiber with the effective refractive index of the core of 1.468 according to the datasheet from the manufacturer. The microwave frequency was chosen to be in the range of 0-6 GHz with 20000 equally-spaced sampling points. 8 weak reflectors with equal reflectivity of 1% were implanted in the fiber at the discrete locations of 0.30, 0.40, 0.60, 0.75, 0.80, 0.90, 1.20, 1.60 m, respectively. The common electrical length of the microwave system was chosen to be 0.20 m.

Figures 2(a) and 2(b) plot the calculated amplitude (A_{eff}) and phase (Φ_{eff}) spectra based on Eq. (11). Figures 2(c) and 2(d) plot the calculated results based on Eqs. (12) and (13), respectively. As shown in Fig. 2(c), the 8 reflectors can be clearly identified at the corresponding locations. A Hanning window function was applied to the time-domain signal shown in Fig. 2(c) to cut out a section including the 4th and 5th reflectors. The center of the Hanning window was located at the center between the two reflectors and the width of the window was chosen to be 1.22 ns. The cut-out section of the time-domain signal was then Fourier transformed back into the frequency domain as shown in Fig. 2(d), where an interferogram can be clearly identified. The reconstructed interferogram is the result of the microwave interference of the two reflected signals at the 4th and 5th reflectors. The FSR was found to be 1.005 GHz, which matched well with that calculated based on Eq. (15).

#212236 - $15.00 USD Received 15 May 2014; revised 15 Jul 2014; accepted 18 Jul 2014; published 25 Jul 2014

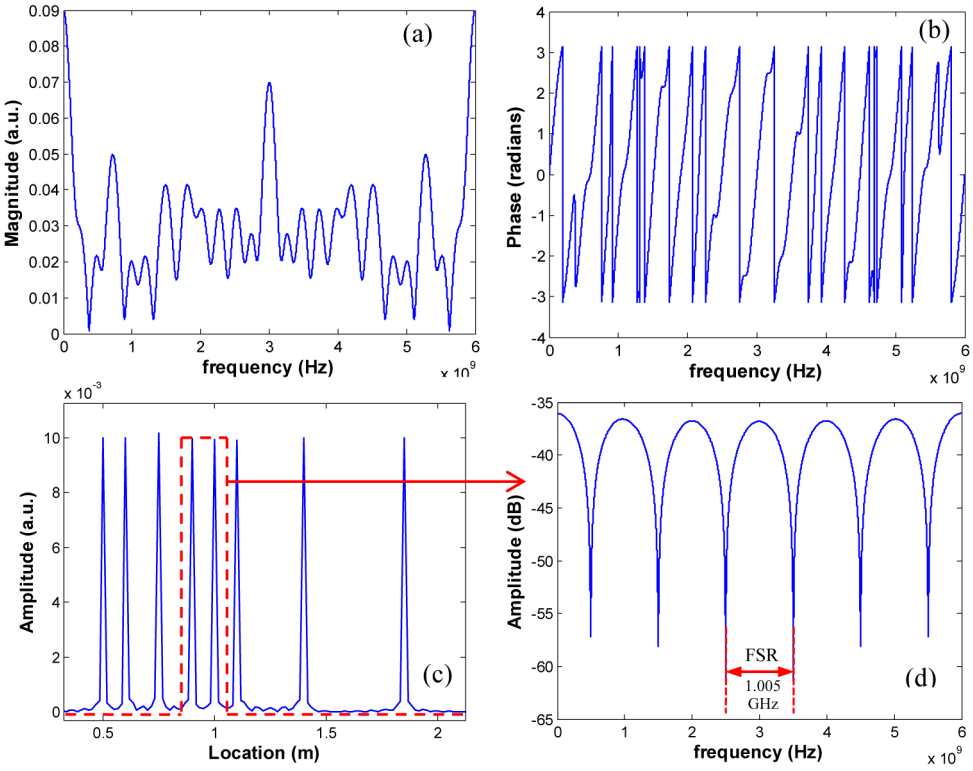

Fig. 2. Simulation of 8 reflectors along a single-mode fiber. The optical reflectivity is equally distributed. The locations of the reflectors are 0.5, 0.6, 0.8, 0.9, 1, 1.1, 1.4, 1.8 m, respectively. (a) Calculated amplitude spectrum (A_{eff}) based on Eq. (11). (b) Calculated phase spectrum (Φ_{eff}) based on Eq. (11). (c) Calculated time/spatial domain result based on Eq. (12). (d) Calculated microwave interferogram of the 4th and 5th reflectors based on Eq. (13).

In a similar way, any two reflectors can be cut out by applying a proper windowing function. In essence, the two cut-out reflectors and the fiber section between them defines a low-finesse fiber intrinsic FPI whose interferogram can be reconstructed in the frequency domain. The reconstructed microwave interferogram can be processed to find its OPD or changes in OPD for sensing applications. The location of the cut-out FPI is also known because the positions of the two reflectors can be found in the time-domain. Spatially continuous distributed sensing can be realized by consecutively selecting two adjacent reflectors along the optical fiber. In addition, any two arbitrary reflectors on the optical fiber can be selected to construct the interferometer. As such, the gauge length can be flexibly reconfigured during measurement.

4. Experimental demonstration

According to the aforementioned modeling and simulation results, the OCMI interferogram of any two reflectors can be unambiguously reconstructed for spatially continuous distributed sensing. To validate the proposed concept, we designed two experiments based on cascaded optical fiber FPIs.

4.1 System implementation

While there are many ways to implement the OCMI concept, Fig. 3 illustrates an example system configuration where a microwave vector network analyzer (VNA) is used as the microwave source and signal detector. A broadband light source with the bandwidth of 50 nm is intensity modulated using an electro-optic modulator (EOM) driven by the microwave

#212236 - $15.00 USD Received 15 May 2014; revised 15 Jul 2014; accepted 18 Jul 2014; published 25 Jul 2014

signal from the Port 1 of a VNA (HP 8753es). The VNA output is DC-biased and amplified to achieve a high modulation index. A fiber circulator is used to route the modulated light into and the output signal out of the distributed fiber optic Fabry-Perot interferometers. An optional erbium doped fiber amplifier (EDFA) can be used for additional signal amplification if needed. After DC-filtering and RF amplification, the photodetector output is connected to the Port 2 of the VNA, where the amplitude and phase of the signal are extracted. By sweeping the VNA frequency, the microwave spectrum (i.e., the S21 of the VNA) of the interferometer is obtained.

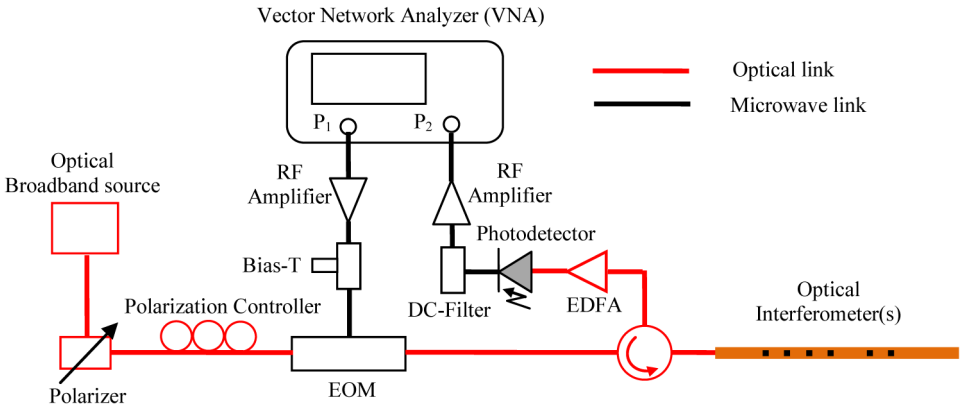

Fig. 3. Schematic of the OCMI system used to support proof-of-concept experiments. A broadband light source (bandwidth ≈50 nm) is intensity-modulated using an electro-optic modulator driven by the microwave output (DC-biased and amplified) from Port 1 of a VNA. The output from the fiber interferometer is detected by a photodetector whose signal, after DC-filtering and RF amplification, is recorded at Port 2 where the amplitude and phase of the signal are extracted. By sweeping the VNA frequency, the microwave spectrum of the interferometer is obtained (i.e., the S21 of the VNA).

4.2 Strain measurement using OCMI-FPIs

As shown in Fig. 4(a), 6 weak reflectors were implemented on a singlemode fiber (SMF-28e) by intentionally misaligning the fibers during fusion splicing. The 6 reflectors divided the entire fiber into 5 measurement sections of different lengths as schematically shown in this Figure. The sensors were interrogated using the OCMI system described in Fig. 3. The microwave interference spectrum of the distributed sensors was first acquired and then complex inverse Fourier transformed to obtain the time resolved reflections along the optical fiber as shown in Fig. 4(b), where the 6 reflections can be clearly identified at the time intervals matching the section lengths. Using a time gating window, we isolated the two reflectors defining Section 3 and reconstructed its microwave interferogram by complex Fourier transform as shown in Fig. 4(c), where interference fringes are clean with the visibility exceeding 25 dB, indicating excellent signal quality. Distributed sensing capability was tested by applying axial strains to Section 3 only. Figure 4(d) shows the zoomed interference fringes at different applied axial strains at Section 3. The fringe moved towards the low frequency regime as the strain increased. Figure 4(e) plots the 3D view of the frequency shift of the interferogram as a function of the applied strain, where the frequency decreases linearly as the strain increases. In contrast, the other sections were left unstressed. As a result, no frequency shifts were observed along the fiber outside Section 3. As shown in Fig. 4(f), the FPI defined by Section 3 had a linear response to the applied axial strain with a sensitivity of - 2.26 KHz/με.

#212236 - $15.00 USD Received 15 May 2014; revised 15 Jul 2014; accepted 18 Jul 2014; published 25 Jul 2014

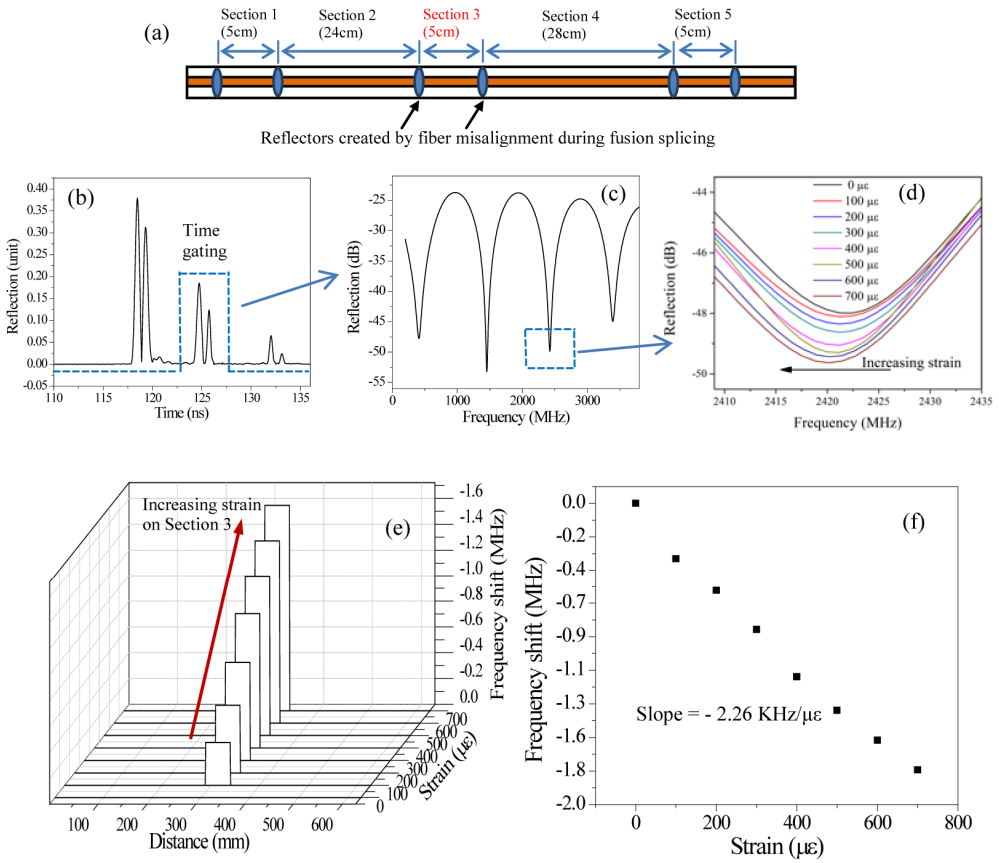

Fig. 4. Validation of the distributed sensing capability of OCMI. (a) SMF distributed sensors with 6 reflectors implanted to divide the entire length into 5 sections, (b) Time resolved reflections along the optical fiber and time gating window to isolate Section 3, (c) Reconstructed microwave interferogram of Section 3, (d) Zoomed interference spectra at different strains, (e) 3D view of the distributed OCMI fiber sensor in response to axial strains applied to Section 3 only, and (f) Frequency shift as a function of the applied strain.

It is worth noting that the reflectors created by fiber misalignments had large losses. As a result, the reflections were not even and their amplitudes dropped quickly. A reflector with controlled reflectivity and negligible losses is needed so that better fringe visibilities can be obtained for each section and the number of reflectors can be significantly increased (thus a much longer monitoring span). Nevertheless, the experiment results clearly show the capability of using OCMI-FPI for strain sensing and the capability of locating the spatial position of the interferometer using the OCMI technique.

4.3 Spatially continuous measurement of distributed strains

We also experimentally validated the spatially continuous distributed sensing capability using cascaded optical fiber intrinsic Fabry-Perot interferometers (IFPI) as illustrated in Fig. 5(a), where 10 weak reflectors were inscribed inside the core of a SMF using femtosecond (fs) laser micromachining. The fs laser is a regeneratively amplified Ti: Sapphire laser (Coherent, Inc.). The central wavelength, pulse width and repetition rate of the laser are 800 nm, 180 fs and 250 kHz, respectively. The maximum output power of the laser is 1 W. The actual power used for fabrication was controlled by adjusting the laser beam optics. The laser operation is fully controlled by a computer. A microscopic video system is included in the system to observe the fabrication process in real time. During fabrication, the lens and fiber were immersed in deionized water. The focused fs laser beam penetrated into the fiber and ablated

#212236 - $15.00 USD Received 15 May 2014; revised 15 Jul 2014; accepted 18 Jul 2014; published 25 Jul 2014

a small cuboid shape with the dimension of 5 μm × 30 μm × 20 μm in the fiber core as shown in Fig. 5(f). The typical reflectivity of such a structure was about −45 dB and the loss was about 0.02 dB measured by an optical power meter. The weak reflectivity and very small loss allow us to cascade many reflectors along a fiber, enabling distributed sensing over a long distance.

The reflectors divided the fiber into 9 consecutive measurement sections. Each section was an IFPI with a length of about 12 cm. The IFPI sensors were epoxied on the surface of an aluminum cantilever beam with its length, width, and thickness of 1,250, 80, and 9.10 mm, respectively. One side of the beam was clamped in a vice. The other side was pushed by a micro-actuator to bend the beam and apply strain to the attached sensors. The distance between the clamp and the micro-actuator was 1.14 m. As the cantilever beam deflected, the amounts of axial strain seen by the IFPI sensors were different. The mathematical model of the cantilever beam used to calculate the strain distribution can be found in [24].

The complex microwave spectrum (amplitude and phase spectrum) of the distributed sensors was first acquired as shown in Figs. 5(b) and 5(c). Then complex inverse Fourier transform was performed to obtain the distance-resolved reflections along the fiber as shown in Fig. 5(d), where the 10 reflections can be clearly identified and their separations match the corresponding section lengths. Using a Hanning window, we isolated the two reflectors defining Section 8 and reconstructed a microwave interferogram by applying complex Fourier transform to the window-gated data. As shown in Fig. 5(e), the reconstructed interferogram is clean and has a visibility exceeding 25 dB.

The deflections of the aluminum plate were increased at a step of 5 cm, measured by a caliper. As the strain increased, the interferogram of each IFPI shifted correspondingly. By tracking the frequency shift of the individual interferogram, the changes in OPDs (thus the physical lengths) were calculated for all the consecutive sections. The strain value of each section was calculated by dividing the physical length change with respect to its initial length calculated based on the FSR of the interferogram. Figure 5(e) shows the measured strains (black dots) of various sections along the cantilever beam at the deflections of 5, 10 and 15 cm, respectively. The measurement data agreed well with the statics model predictions, i.e., the mesh grids in Fig. 5(g). The strain increased at the location that was closer to the clamped end of the beam. The strain also increased at the same location as the deflection increased.

In our preliminary OCMI system, the microwave bandwidth was about 6 GHz, which provided a theoretical spatial resolution of about 3 cm. The pulses shown in Fig. 5(d) indicated no obverse overlap for the reflectors separated by about 12 cm. Given that modern microwave instrumentation can easily reach 50 GHz bandwidth, the spatial resolution can be as high as a few millimeters.

#212236 - $15.00 USD Received 15 May 2014; revised 15 Jul 2014; accepted 18 Jul 2014; published 25 Jul 2014

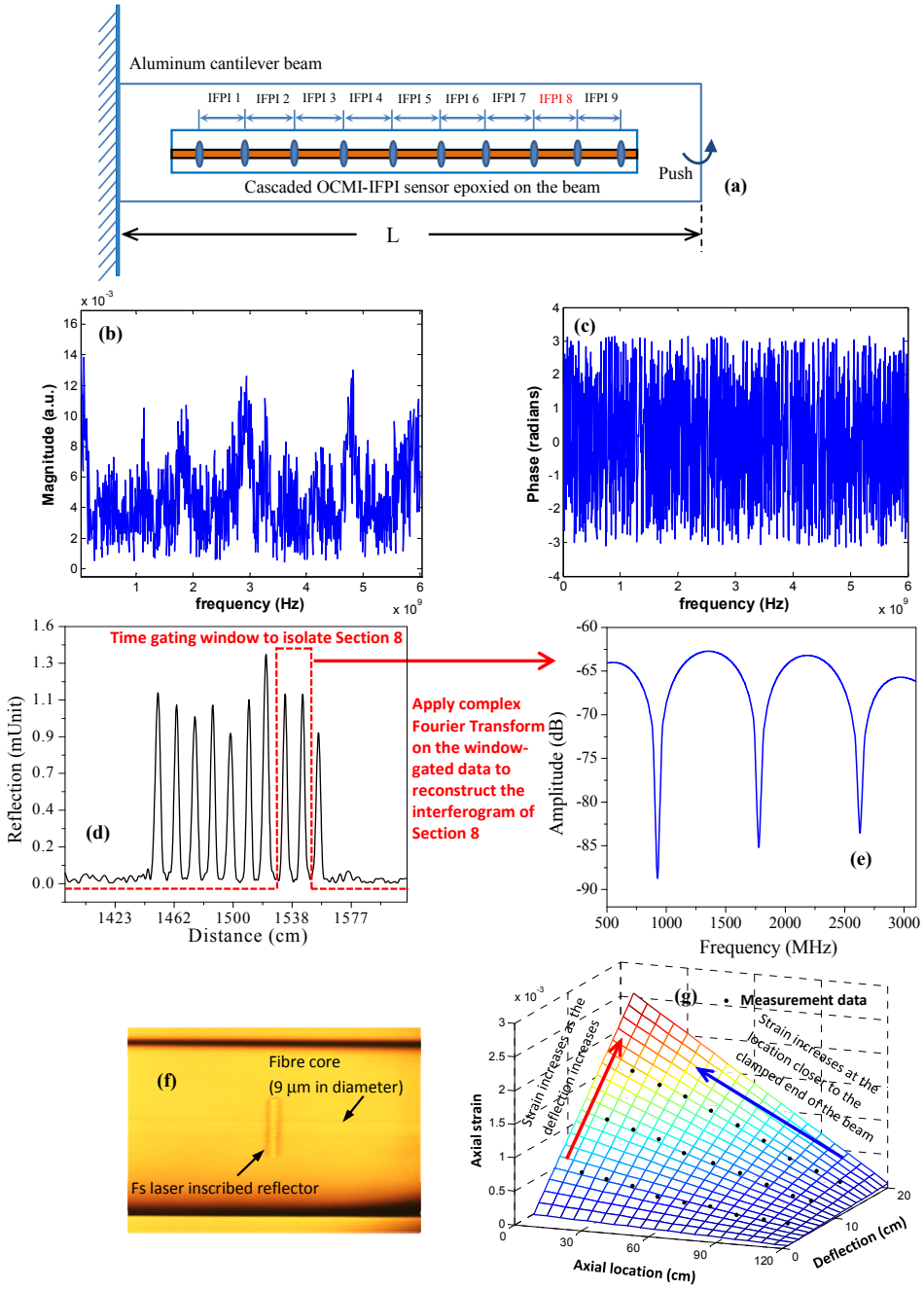

Fig. 5. (a) Schematic illustration of the experiment setup to validate the distributed strain sensing capability of OCMI. (b) Amplitude spectrum and (c) phase spectrum of the distributed sensor systems. (d) Time/distance resolved reflections along the optical fiber where the 10 weak reflections can be clearly identified with excellent SNR. (e) Reconstructed microwave interferogram of Section 8. (f) Confocal microscopic image of a weak reflector fabricated by femtosecond laser micromachining. Using water immersion fabrication, the focused fs laser beam penetrated into the fiber and ablated a very small region inside the fiber core. The reflector has a typical reflectivity of about –45 dB and a typical loss of about 0.02 dB. (g) Measured strain distribution at the different sections along the beam under different amounts of deflections.

#212236 - $15.00 USD Received 15 May 2014; revised 15 Jul 2014; accepted 18 Jul 2014; published 25 Jul 2014

6. Conclusion

In conclusion, a new distributed fiber optic sensing technique using optical carrier based microwave interferometry was developed. Many optical interferometers with the same or different optical path differences are interrogated in the microwave domain and their locations can be unambiguously determined. The concept is demonstrated using cascaded weak optical reflectors along a single optical fiber, where any two arbitrary reflectors are paired to define a low-finesse Fabry-Perot interferometer. Spatially continuous (i.e., no dark zone), fully distributed strain measurement was used as an example to demonstrate the capability of the proposed concept. The spatial resolution is inversely proportional to the microwave bandwidth. With a microwave bandwidth of 6 GHz, the spatial resolution can reach 3 cm. Although distributed strain measurement using cascaded FPIs was used as a demonstration, the proposed concept may also be implemented on other types of waveguide or free-space interferometers. In addition to strain measurements, it can also be flexibly designed to measure other physical, chemical and biological quantities by encoding the parameters to be measured into the OPDs of the interferometers. As presented in [21], by reading the fiber optic interferometers in microwave domain, the system offers many unique features including high signal quality, relieved requirement on fabrication, low dependence on the types of optical waveguide, and insensitivity to the variations of polarization. It is also envisioned that the proposed technique could be implemented in special optical fibers (e.g., multimode, single crystal sapphire and polymer fibers), optical waveguides and free space. The new distributed sensing concept may enable many important applications that are long-desired but currently unavailable.

Acknowledgments

The authors acknowledge funding supports from Department of Energy, National Energy Technology Laboratory, under Contract Number DE-FE0012272, and National Science Foundation CMMI-1359716.

#212236 - $15.00 USD Received 15 May 2014; revised 15 Jul 2014; accepted 18 Jul 2014; published 25 Jul 2014